

# Automated calculation of the axial orientation of intravascular ultrasound images by fusion with biplane angiography

Andreas Wahle,<sup>a</sup> Guido P. M. Prause,<sup>ab</sup> Clemens von Birgelen,<sup>c</sup>  
Raimund Erbel,<sup>c</sup> and Milan Sonka<sup>a</sup>

<sup>a</sup> The University of Iowa, Department of Electrical and Computer Engineering,  
Iowa City, IA 52242-1527, USA

<sup>b</sup> MeVis Institute at the University of Bremen,  
D-28359 Bremen, Germany

<sup>c</sup> University Hospital Essen, Medical Clinic, Department of Cardiology,  
D-45122 Essen, Germany

## ABSTRACT

This paper presents an approach for fusion of the two major cardiovascular imaging modalities, angiography and intravascular ultrasound (IVUS). While the path of the IVUS catheter, which follows the vessel curvature during pullback, is reconstructed from biplane angiograms, cross-sectional information about the vessel is derived from IVUS. However, after mapping of the IVUS frames into their correct 3-D locations along the catheter path, their orientations remain ambiguous. We determine the relative catheter twisting analytically, followed by a statistical method for finding the absolute orientation from the out-of-center position of the IVUS catheter. Our results as obtained from studies with cadaveric pig hearts and from three patients undergoing routine coronary intervention showed a good match of the absolute orientation by the algorithm. In all tested cases, the method determined the visually correct orientations of the IVUS frames. Local distortions were reliably identified and discarded.

**Keywords:** 3-D reconstruction, multimodal fusion, coronary artery system, quantitative analysis, biplane angiography, intravascular ultrasound, catheter twist, absolute orientation.

## 1. INTRODUCTION

While intravascular ultrasound (IVUS) gains increasing importance,<sup>1-4</sup> assessment of vasculature still lacks a geometrically correct 3-D reconstruction. The IVUS frames are usually stacked up to form a straight vessel, thus resulting in distorted interpretation and quantification.<sup>5</sup> Our approach combines the advantages of IVUS with those of biplane angiography, namely obtaining the vessel curvature from the angiographic projections, while the vessel cross-sections are analyzed from the IVUS data (Fig. 1). The 3-D catheter path as well as the vessel lumen borders are reconstructed automatically from their angiographic projections using a previously developed method.<sup>6,7</sup> The IVUS images are segmented to yield wall and plaque borders using our well-established graph-search approach.<sup>8</sup>

The problem of assigning the IVUS data into 3-D space is two-fold: 1) They have to be related to 3-D locations, and 2) their orientations have to be determined. Early approaches identified the location of the transducer—and thus of the respective IVUS image—by constant angiographic supervision during the pullback,<sup>9,10</sup> which is accurate but not acceptable in clinical routine. Using a constant pullback speed, which can be assured by automated devices, the location of each IVUS frame can be derived from the time function of the pullback.<sup>11</sup> Another complex task is the identification of the spatial frame orientation. The *relative* changes in orientation between adjacent IVUS frames are determined analytically based upon the Frenet-Serret rules.<sup>12,13</sup> However, the *absolute* orientation in 3-D remains ambiguous. The problem is comparable to fitting a sock on a leg.<sup>14</sup> While the leg (catheter path) is stable, the sock (axial frame orientation) can freely be rotated around the leg, but fits optimally only in one orientation. Current approaches either try to match the IVUS contours with the angiographic profiles by backprojection,<sup>15</sup> or rotating the entire set interactively until the images approximately match the angiographic outline.<sup>14</sup> The use of branches as natural landmarks is frequently unreliable since their origins may be difficult to identify with sufficient accuracy in both angiograms and IVUS images.<sup>16</sup>

---

E-mail: <andreas-wahle@uiowa.edu>; supported in part by *Deutsche Forschungsgemeinschaft*, Germany (Pr 507/1-2, Wa 1280/1-1)

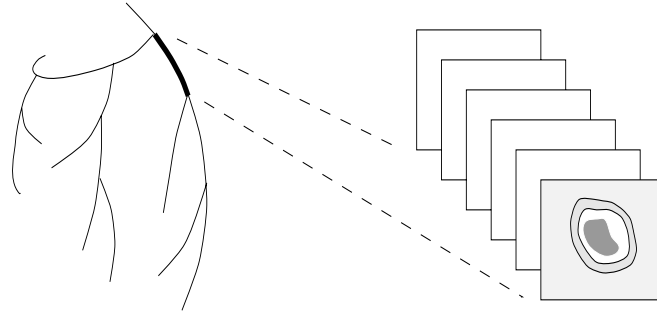


**Figure 1.** Fusion approach; the IVUS frames are mapped on the 3-D trajectory of the imaging catheter.

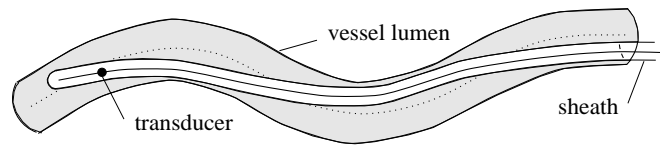


**Figure 2.** Bending of the imaging catheter within the vessel due to vessel curvature; the catheter is seeking a position of minimum energy.

We present a new method for automated determination of the absolute orientation using the bending behavior of the imaging catheter as a reference, which is expected to fall in the position of minimum energy within the vessel (Fig. 2). In both angiograms and all IVUS frames, the *out-of-center position* of the catheter relative to the inner lumen is analyzed (Fig. 3). Using a non-iterative statistical approach, the optimum fit of the IVUS frame set is calculated.

## 2. METHODS

The outline of the system is displayed in Figure 4. First, the 2-D *catheter path* and *vessel outline* are extracted from both angiograms and then reconstructed to a 3-D model. From the 3-D catheter path, the *relative catheter twist* can be estimated and serves as a basis for the relation between adjacent IVUS frames. The *lumen* is segmented in both IVUS image data and angiograms, where the angiographic lumen is represented in 3-D by elliptical contours derived from the 2-D outlines. In both data sets, the *out-of-center position* of the imaging catheter relative to the lumen is determined. Then, the IVUS data is mapped into 3-D using an *initial orientation* along with the relative twist. For each frame location, the *out-of-center strength* and the *difference angles* of angiographic vs. IVUS reconstruction are determined. Within a *moving window* of arbitrary but fixed size, a statistical analysis is performed. A *reliability weight* is calculated for each location of the moving window, giving higher weight to locations with high out-of-center strength, and limiting those with a high standard deviation of the difference angle function, which is indicating local distortions. A single *correction angle* is determined and applied to all IVUS frames relative to the initial orientation.

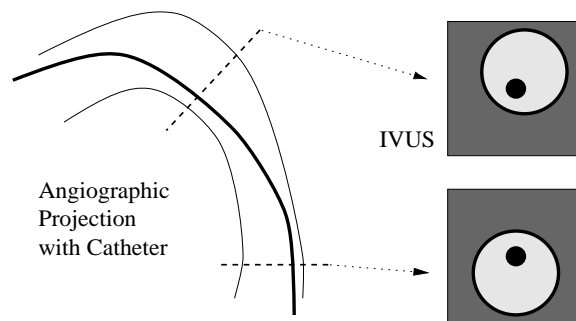


**Figure 3.** Appearance of out-of-center position of the imaging catheter in angiographic and IVUS images.

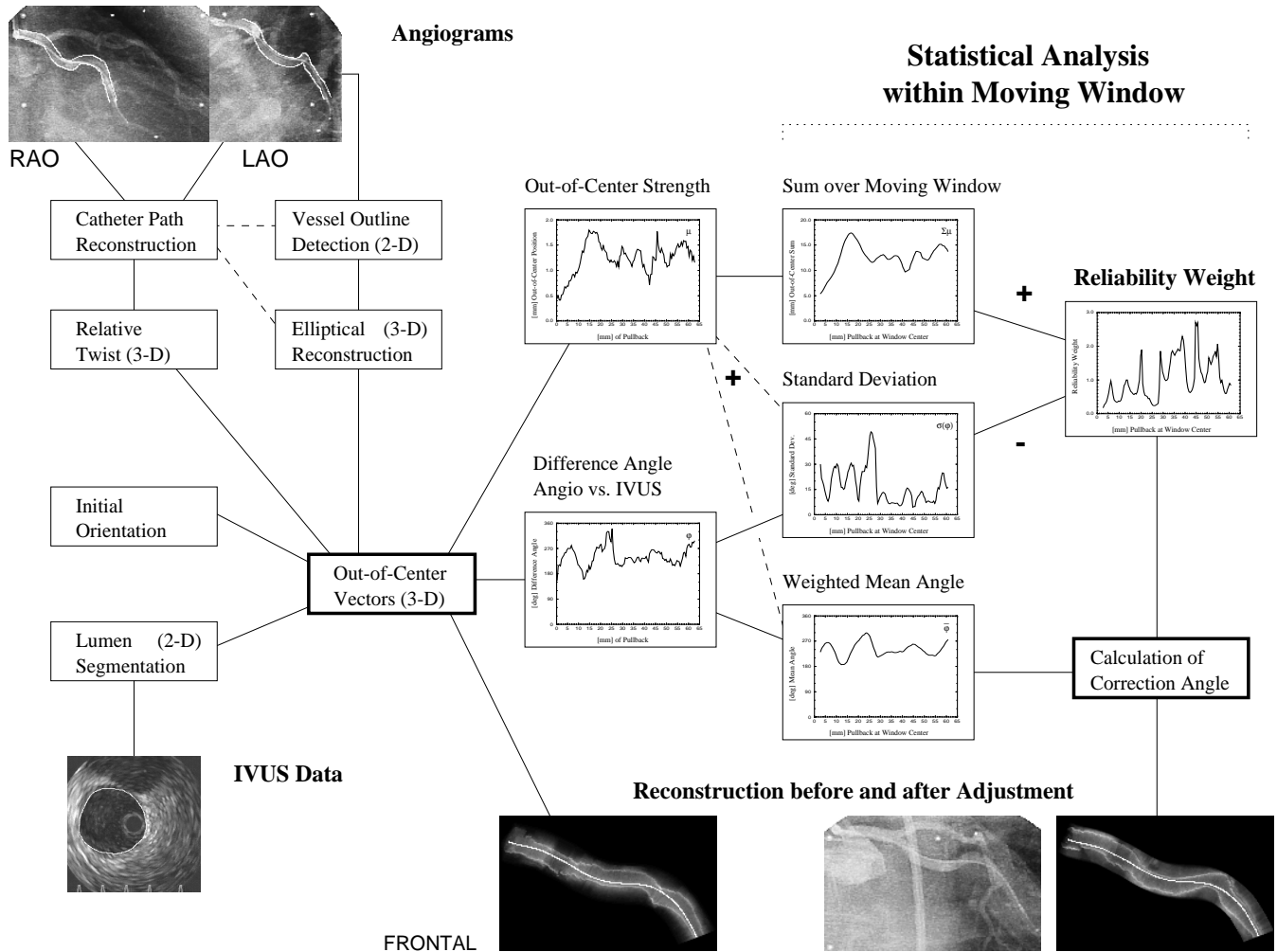


Figure 4. Flow-chart for the fusion approach (see text for details).

### 2.1. 3-D Catheter Path and Vessel Outline

The biplane angiograms used for extraction of the catheter path as well as the vessel outline are taken immediately before pullback start and are corrected for geometric distortions in a preprocessing step.<sup>16</sup> After the catheter path is determined by applying a dynamic programming approach,<sup>17</sup> it is used as a guide line for the detection of the vessel borders by a modified version of the algorithm of Beier.<sup>18</sup>

From the known imaging geometry, both catheter path and vessel outline are reconstructed using the method previously developed and validated at the German Heart Institute of Berlin.<sup>6,7</sup> The projection rays of corresponding points (e.g. the transducer tip) can be reconstructed into 3-D space, and — with respect to the epipolar constraint — the original 3-D location of the point reconstructed at the minimum distance between these rays. The calculation of the rays depends on the assumed imaging geometry. Two contrary concepts of determining the imaging geometry exist: Either it is calculated analytically from the gantry parameters,<sup>19</sup> or it is obtained from imaging a calibration object.<sup>20</sup> Newer approaches calculate a relative description between the two gantries from a set of corresponding reference points without any calibration object.<sup>21,22</sup> Our system utilizes the available gantry parameters for an initial geometry, which is then refined using 2–5 corresponding points in the angiograms as reference.<sup>6,7</sup>

Along the extracted path of the catheter, corresponding elements are found using the epipolar constraint.<sup>23,24</sup> The reconstruction yields a combined 3-D model of the catheter and the vessel lumen for each of these elements, where the lumen is restricted to elliptical cross-sectional shapes.<sup>6,7</sup>

## 2.2. IVUS Frame Location Matching

For an IVUS catheter with a sheathed design,<sup>1,2</sup> the location of the catheter as shown in the angiograms before pullback start indicates the path of the catheter core during the pullback, since the sheath remains in its position while only the core is moved (Fig. 2). From the time-stamps of a specific frame vs. the frame at pullback start, along with the known speed of the pullback, the distance of this frame to the start frame on the catheter trajectory can be calculated.<sup>11</sup>

However, as we could show earlier, the manual pullback is affected by unavoidable tolerances and thus cannot be treated as constant-speed.<sup>25</sup> Using an automated pullback device ensures a proper matching of the frame. After identification of the 3-D locations, the angiographically determined elliptic contours are assigned to their corresponding IVUS frames.

## 2.3. Frame-to-Frame Relative Orientation

The *catheter twist* is defined as the relative axial changes of the catheter orientation when the catheter is influenced by vessel curvature and torsion.\* The relative twist between adjacent IVUS frames is calculated using our sequential triangulation method described in detail elsewhere.<sup>13,16</sup>

From the orientation of the previous frame and the local path of the catheter, the orientation of the next frame is calculated by a discrete version of the Frenet-Serret<sup>12</sup> rules. Using the three points of the catheter path next to the two adjacent frames, a circumscribing circle is calculated. The sector between the two images is considered a part of the circle. Thus, the new frame is calculated by rotating the previous frame around the normal  $n_i$  of the circle by the enclosed angle  $\alpha_i$  (Fig. 5). This algorithm has been extensively validated in phantom studies.<sup>13,16</sup>

## 2.4. Initial Orientation of the Frame Set

The estimation of the absolute orientation is based on error minimization. Since no indication of the IVUS frame orientation is available at the beginning of the process, the frames are first mapped into 3-D space using an *initial orientation*. The reconstruction error is calculated from the out-of-center vectors, indicating magnitude and orientation, and then a correction angle relative to the initial orientation is generated.

The initial orientation is obtained from the orientation of a reference plane, which was already introduced for the evaluation of the relative twist.<sup>26</sup> This plane is calculated by bilinear regression from the set of catheter elements as reconstructed from the angiograms. The horizontal axis of the first IVUS frame is then oriented parallel to this reference plane, while the axes of the subsequent IVUS frames are oriented with respect to the relative twist as determined before.

## 2.5. Calculation of the Out-of-Center Vectors

From the angiograms, the out-of-center vectors can directly be determined using the reconstructed elliptical contours and the catheter trajectory. The intersection of the catheter path with the generated ellipse is determined at the level of the corresponding IVUS frame. The out-of-center vector is then calculated as the 3-D vector beginning at this intersection point and ending at the center of the ellipse.

For the IVUS frames, the determination of the center point is more complex since the contour may have a free shape. Assuming a homogeneous distribution of the contour points, the centroid for contour  $j$  containing  $n_j$  points  $[u_{ij}, v_{ij}]$  is calculated by

$$S_j = [\bar{u}_j, \bar{v}_j] = \frac{1}{n_j} \sum_{i=0}^{n_j-1} [u_{ij}, v_{ij}] \quad (1)$$

The location of the catheter within the 2-D image is fixed, usually at the center of the image. Both centroid and catheter points are mapped into 3-D by using the frames reconstructed with the initial orientation. Again, the 3-D out-of-center vector is the vector beginning at the catheter point and ending at the mapped centroid of the contour.

The application of the IVUS lumen contour requires a previous segmentation. This is performed in a semi-automated process using heuristic graph search on a frame-by-frame basis. Our algorithm has been validated previously and proven to be reliable.<sup>8</sup>

---

\* as defined by differential geometry.

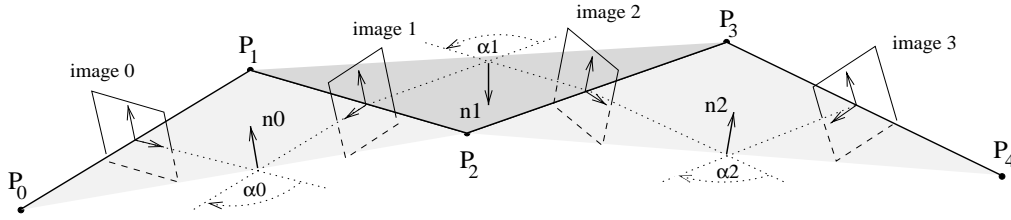


**Figure 5.** Sequential triangulation algorithm for calculation of catheter twist.

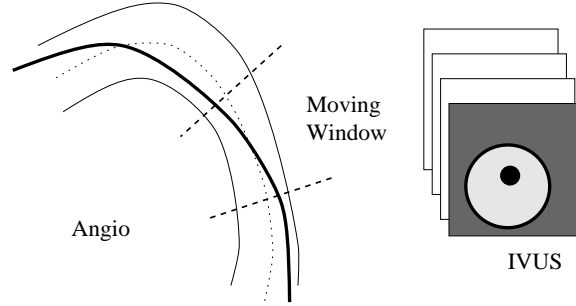


**Figure 6.** Determination of the out-of-center vectors, dotted line represents the centers of the elliptical contours reconstructed from the angiograms; correction angles are sampled within fixed-sized and overlapping moving windows.

## 2.6. Error Minimization

For each of the IVUS frames, the out-of-center magnitude and orientation are determined in both angiographic and IVUS data. The magnitude  $\mu$  is calculated as the length of the out-of-center vector in the IVUS data set, where the in-plane resolution is much higher than in angiography. The difference angle  $\varphi$  is calculated as the inclination angle between the angiographically reconstructed out-of-center vector and the one mapped from the respective IVUS image.

The correction process is a statistically based optimization that incorporates several weighting mechanisms. Due to local tolerances, either from the reconstruction process, slight mismatches in IVUS localization, resolution, etc., the weighting does not only include the effect strength  $\mu$ , but also the *reliability* of the local data, i.e. the variances of the difference angle function  $\varphi$ . This is performed by analyzing the data within a moving window of an empirically determined fixed size along the catheter path (Fig. 6).

Within the window, each difference angle  $\varphi$  is weighted by the vector length  $\mu$ . For each window  $k$ , the weighted mean  $\bar{\varphi}_k$  and the weighted standard deviation  $\sigma(\varphi_k)$  of the difference angle as well as the sum of weights  $\Sigma\mu_k$  are derived. After those values have been determined for all locations of the moving window, the correction angle is calculated from the values over all windows. The positive weight (i.e. locations with increased significance for the estimation of the correction angle) is the sum of weights  $\Sigma\mu_k$ , while the negative weight (i.e. locations with distorted out-of-center data) results from the local tolerances  $\sigma(\varphi_k)$ . The correction angle results from the weighted mean

$$\bar{\varphi}_{\text{corr}} = \sum_k \left( \bar{\varphi}_k \frac{\Sigma\mu_k}{\sigma(\varphi_k)} \right) / \sum_k \left( \frac{\Sigma\mu_k}{\sigma(\varphi_k)} \right) \quad (2)$$

and is to be applied to all IVUS frames.

## 3. RESULTS

### 3.1. In-Vitro Validation

The fusion approach was validated in a series of in-vitro studies using computer models, phantoms, and cadaveric pig hearts.<sup>13,27,28</sup> For the accuracy assessment of our absolute orientation method, we used a cadaveric pig heart that was immersed in a water bath and filled with diluted contrast dye for angiography. Manual IVUS pullbacks of approx. 100mm were performed using a mechanically driven 2.9F 30MHz catheter. The catheter path and the vessel outline were extracted from the angiograms (Figs. 7a/b), vessel lumen and wall borders segmented

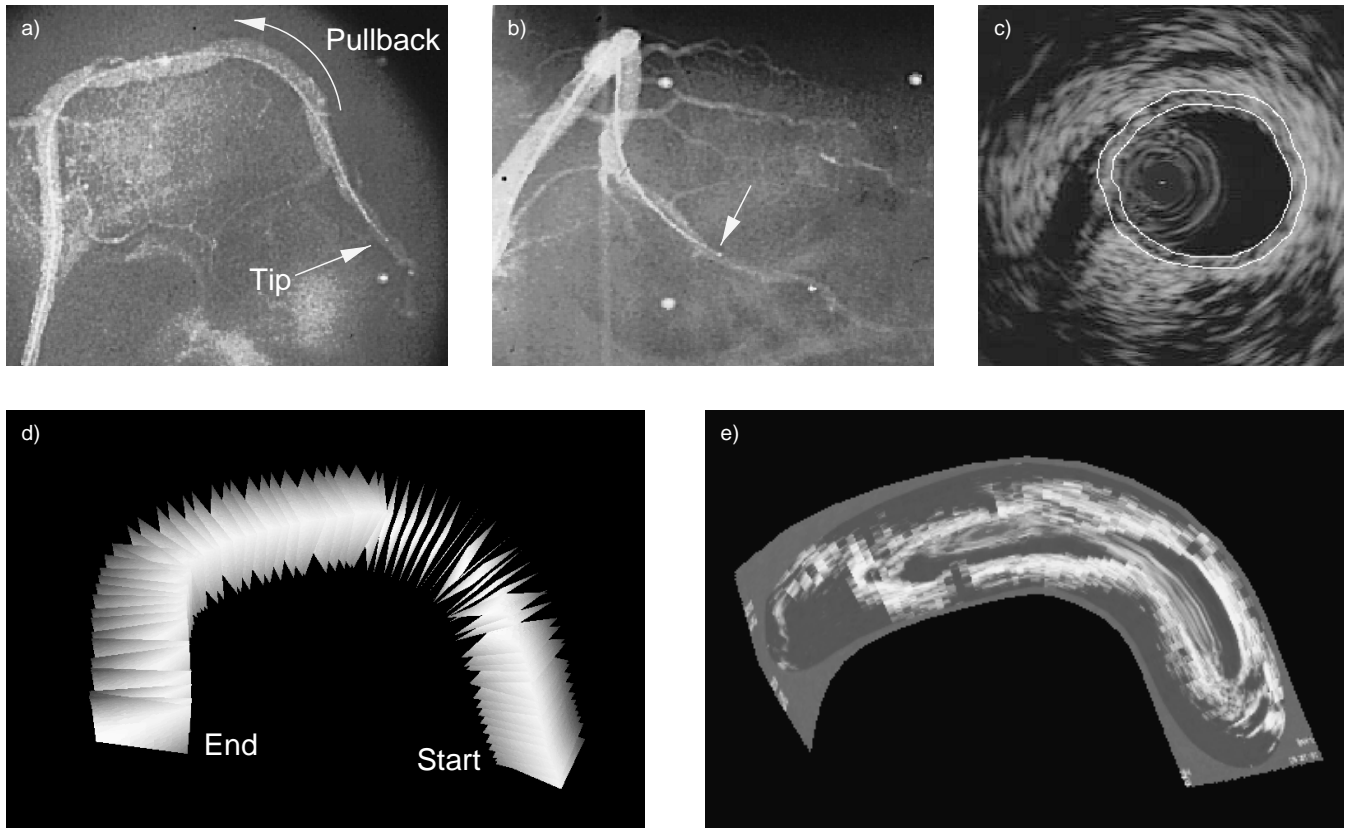


**Figure 7.** a) Frontal and b) lateral angiograms of a cadaveric pig heart with catheter inserted; c) automatic detection of the laminae borders in one of the IVUS images, note the out-of-center position of the catheter; d) VRML scene showing the spatial location and relative orientation of the IVUS frames; e) longitudinal slice through the reconstructed voxel cube, compare the catheter position with that in the frontal angiogram.

from IVUS (Fig. 7c), and after calculation of the frame orientations (Fig. 7d), the IVUS data were mapped into 3-D space, generating a volume model (Fig. 7e). The algorithm could identify the relevant areas reliably, e.g. the arcs where the catheter hits the inner side of the vessel, as well as the straight part where the catheter hits the outer side of the vessel.

Due to inhomogeneous speed of the manual pullback,<sup>25</sup> several localization errors occurred, especially within the first (distal) half of the pullback. While small deviations are detected from high local tolerances, resulting in a strongly reduced weight, longer segments exceeding the size of the moving window may falsely seem to be reliable. In the given example, these errors occurred in the distal arc. Compare the respective segment between the frontal angiogram (Fig. 7a) and the IVUS reconstruction (Fig. 7e). This matching error of about 15 mm resulted in an axial mismatch of  $33.6^\circ$  compared to the proximal part, which was considered to be accurate by visual comparison. After increasing the width of the moving window from 10 mm to 25 mm, the difference was reduced to  $14.7^\circ$ . Discarding the distorted subsegment, i.e. setting  $\mu = 0$  for the involved out-of-center vectors over a length of 15 mm, reduced the mismatch to  $9.4^\circ$  for 10 mm window width.

Since the proximal part seems undistorted, we focused the evaluation on locations 48–102 mm of the pullback (Figs. 8–10). The out-of-center position  $\mu$  shows several minor peaks, while the difference angle  $\varphi$  is stabilizing from distal to proximal. Applying the moving window, the out-of-center sum  $\Sigma\mu_k$  is almost constant with a tendency to higher values towards the end of the pullback, and the standard deviation  $\sigma(\varphi_k)$  is clearly decreasing. Consequently, the reliability weight function (Fig. 10) increases in the proximal window locations. Note that the remaining high tolerances due to the mismatches (50–55 mm) are successfully discarded, while a local peak (58–60 mm) resulted from a temporary stabilization of the difference angle function around  $\varphi = -90^\circ$ .

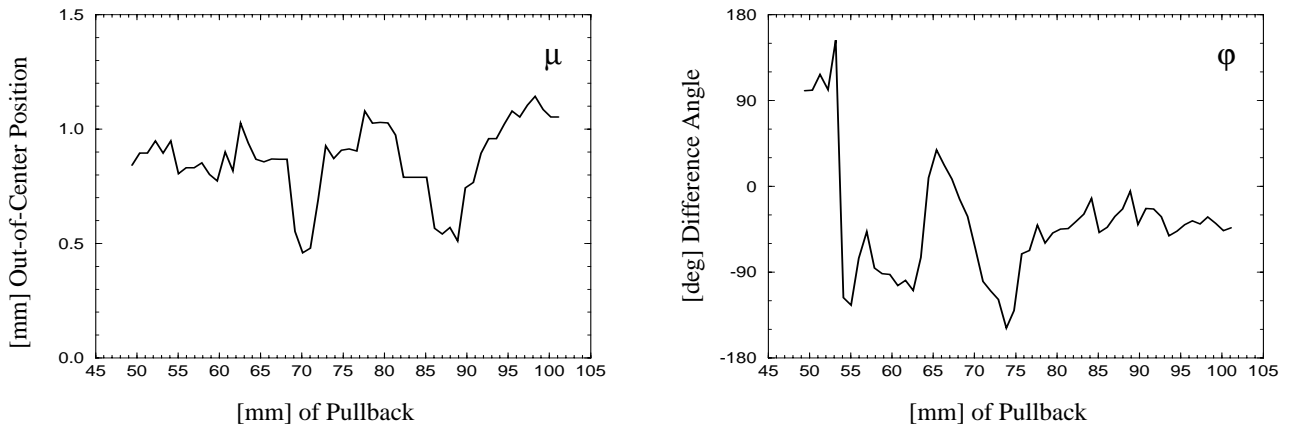


**Figure 8.** Functions for length  $\mu$  of the out-of-center vector and local correction angle  $\varphi$  determined from initial orientation, for each IVUS image, for the proximal part of the cadaveric pig artery shown in Figure 7.

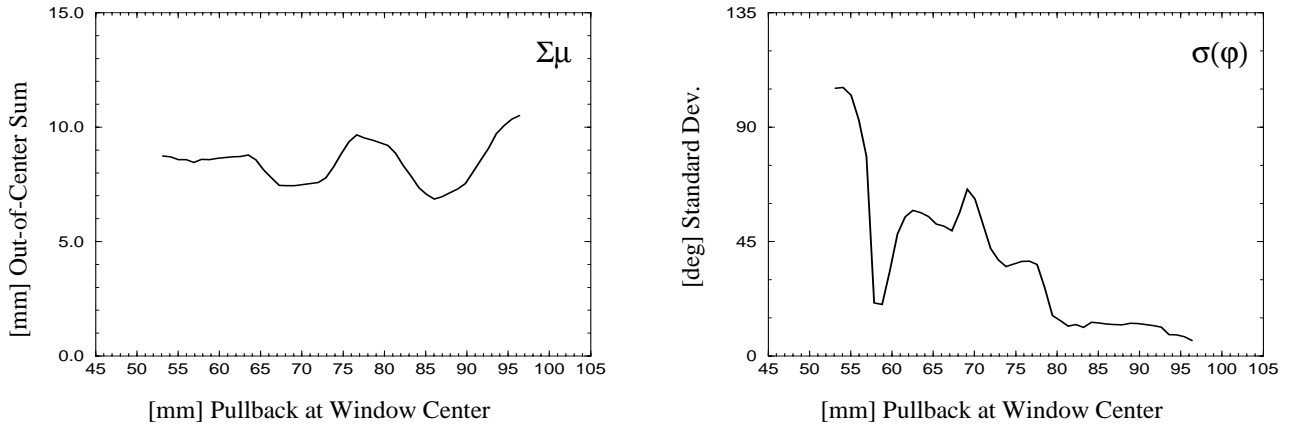


**Figure 9.** Derived values for sum of weights  $\Sigma\mu_k$  and weighted standard deviation  $\sigma(\varphi_k)$ , for each location of the moving window with a size of 10 mm.

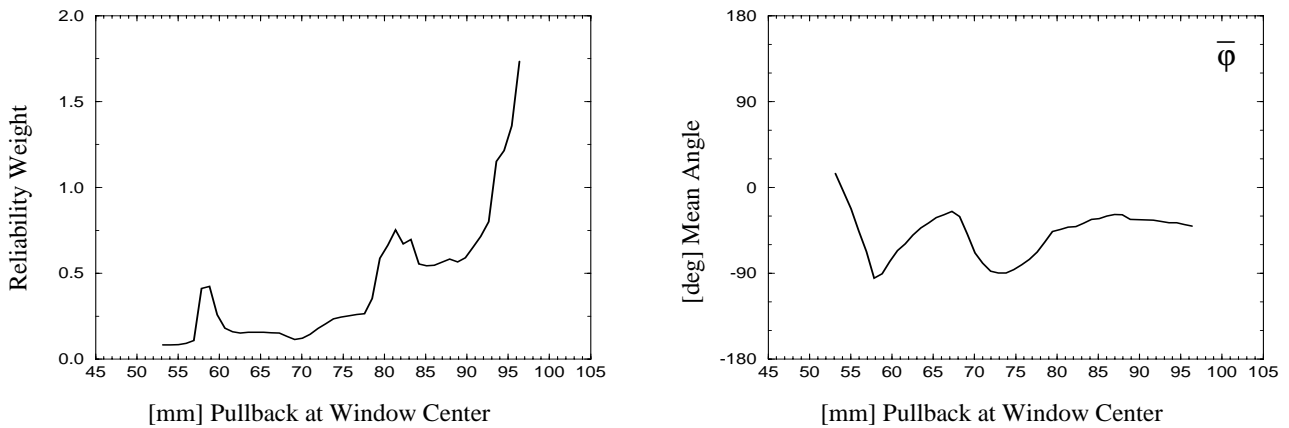


**Figure 10.** Final functions for reliability weight  $\Sigma\mu_k/\sigma(\varphi_k)$  and weighted mean difference angle  $\bar{\varphi}_k$ , for each location of the moving window, used for the calculation of the correction angle.

### 3.2. In-Vivo Application

Up to now, the approach was applied to three patients with stable coronary artery disease, undergoing coronary revascularization and stent placement in native coronary arteries, and which were imaged as part of their clinical procedure. The visually correct orientations of the IVUS frames were found in all cases. An example of a stenosed left anterior descending artery is shown in Fig. 11, with a segment of 40 mm evaluated. The biplane angiograms were acquired both at the beginning and at the end of each pullback at a biplane Siemens HICOR cath-lab with DICOM output on CD-R. Sheathed 2.9F and 3.2F 30MHz catheters (Boston Scientific, San Jose, CA) and automated pullback with a constant speed of 0.5 mm/s were used for IVUS imaging.

As can be seen from Fig. 12, the out-of-center strength  $\mu$  varies between a peak in the second quarter of the pullback (10–20mm) and values below angiographic resolution. The difference angle function  $\varphi$  is most stable at the peak, while it is almost random at the location with low out-of-center strength. Thus, the second quarter was automatically assigned the highest weight for the determination of the absolute orientation. Some possible sources for distortions can be identified from this example: At the beginning of the pullback, a slight wobbling of the catheter can be seen, and the stenotic part suffered from a differently reconstructed shape from angiograms vs. ultrasound. Both zones were successfully identified and discarded, along with the zones that contain minimal out-of-center information.

To estimate the effect of the width of the moving window, the vessel was analyzed with three different window sizes (Fig. 13). The smaller the window size, the higher are the peaks. As expected, increasing the window width results in smoothing of both the reliability weight and the mean angle functions. However, the curves for a width of 12.5 mm are not simply the result of smoothing the curves for a width of 5.0 mm by the respective ratio. While the difference of the resulting correction angle was  $20.4^\circ$  between 5.0 and 7.5 mm window widths, it was just  $2.8^\circ$  between 7.5 and 12.5 mm window widths.

## 4. DISCUSSION

Along with our previously developed and validated methods for geometrical 3-D reconstruction from biplane angiograms,<sup>6,7</sup> border segmentation from intravascular ultrasound,<sup>8</sup> and analytical calculation of the catheter twist,<sup>13,16</sup> the presented method has a high potential to overcome a major problem in the determination of the absolute orientations of the IVUS frames. Using the catheter itself as an artificial landmark does avoid the need for detecting frequently unreliable natural landmarks or the application of markers directly on the vessel.

However, like other methods working on angiographic or ultrasound image data, some limitations are obvious: The use of manual pullback, as well as any manual handling of the imaging catheter during acquisition, introduces mismatches in the localization of the IVUS frames and artificial superimposed twist.<sup>25</sup> When mechanically driven catheters are used, additional distortions are caused by phase shifts along the rotating core.<sup>28</sup> A general problem of angiography is the possible foreshortening, which occurs whenever a specific vessel segment is not oriented orthogonal to both projections.<sup>29,30</sup> Despite the fact that our method is considering ambiguities in the reconstruction of the ellipses,<sup>6,7</sup> foreshortening should be minimized to allow optimal performance of our algorithm for the determination of the absolute orientation. Strong foreshortening can even result in a distorted reconstruction of the catheter path, since ambiguities in the assignment of corresponding path elements between the projections may occur.<sup>24,31</sup> Several methods to detect and to correct inappropriate imaging geometries have been proposed to avoid this problem, either by using visual guidance,<sup>32</sup> or by analytical adaptation of the gantry parameters.<sup>30,33–35</sup>

The developed system has shown to be robust against the above problems, and misinterpretations occur only in severe cases, e.g. if a distorted area is consistent within a width of the moving window, thus impeding a detection by the reliability weight. The analysis of the calculated function for the difference angles concerning systematics should be straightforward and will further help to detect and discard distorted areas.

## 5. CONCLUSION

We reported a comprehensive approach to fusion of intravascular ultrasound and biplane angiography, based upon usage of IVUS catheters in sheathed design. We presented a new method for determining the absolute orientation of the IVUS frames in 3-D. This method uses the out-of-center position of the IVUS catheter as a reference. By the introduction of a reliability weight along with a moving window technique, possible errors are successfully detected and discarded. Thus, our system delivers a high-quality reconstruction of the IVUS data, and allows geometrically correct analyses of coronary vessels. The presented fusion approach operates on a highly automated level and substantially improves the clinical applicability of cath-lab imaging.



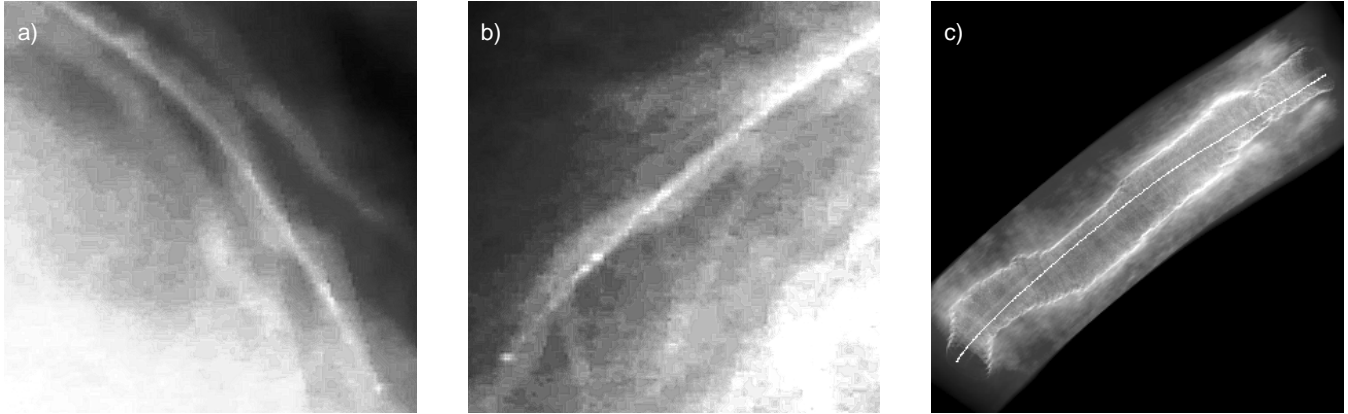


**Figure 11.** Detail in a) 30° right and b) 60° left anterior oblique projections of an in-vivo acquisition of the left anterior descending artery; c) transmission image through the generated voxel cube in lateral view, catheter location and segmented lumen borders have been marked in the 2-D IVUS images before mapping.

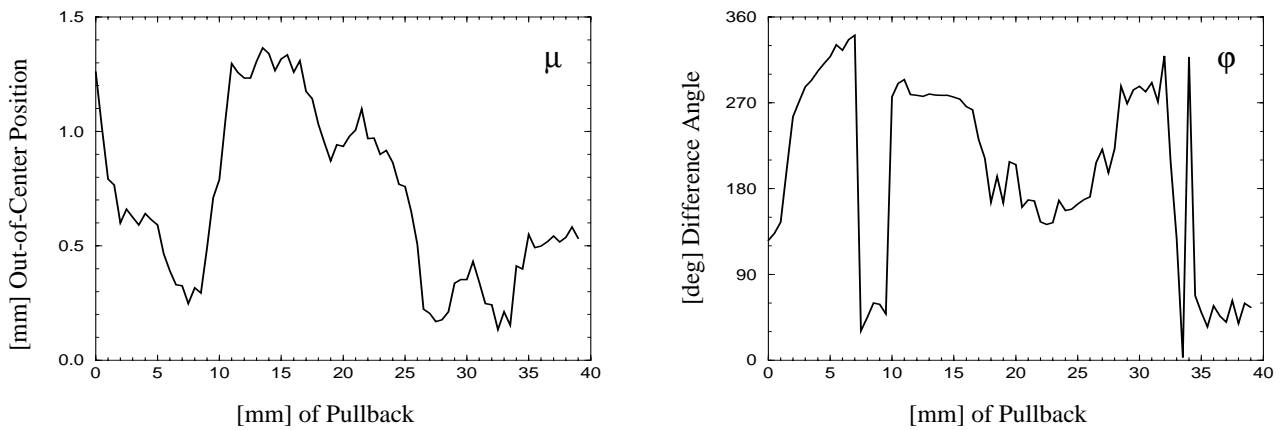


**Figure 12.** Functions for length  $\mu$  of the out-of-center vector and local correction angle  $\varphi$  of the human artery shown in Figure 11; note the high variances in the angle function when the out-of-center position falls below angiographic resolution ( $<0.5$  mm).

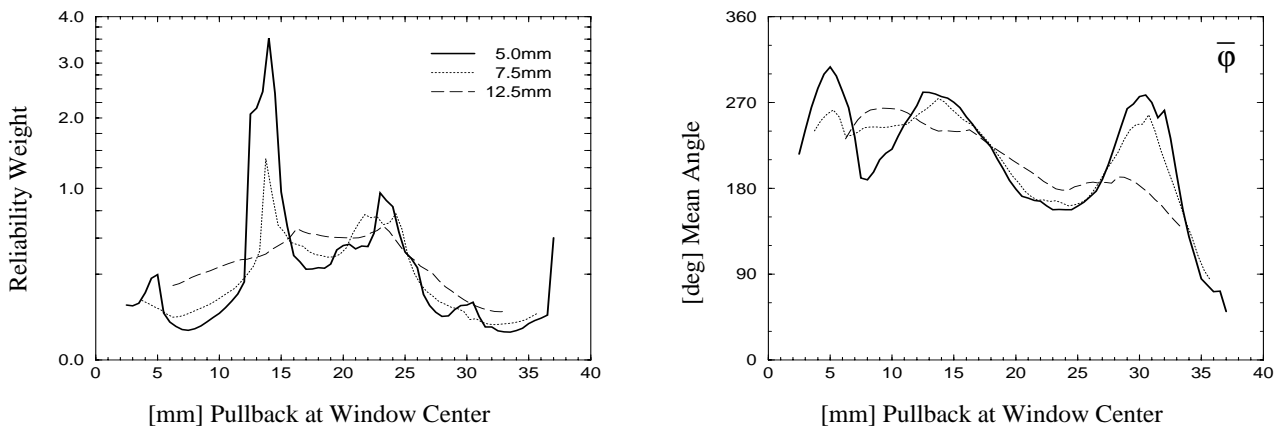


**Figure 13.** Final functions for reliability weight  $\Sigma\mu_k/\sigma(\varphi_k)$ , with non-linear scale to allow a better visual comparison of the curves, and weighted mean difference angle  $\bar{\varphi}_k$ , for each location of the moving window in three different sizes.

## REFERENCES

1. C. von Birgelen, G. S. Mintz, P. J. de Feyter, N. Bruining, A. Nicosia, C. D. Mario, P. W. Serruys, and J. R. T. C. Roelandt, "Reconstruction and quantification with three-dimensional intracoronary ultrasound; an update on techniques, challenges, and future directions," *European Heart Journal* **18**, pp. 1056–1067, July 1997.
2. C. von Birgelen, E. A. de Vrey, G. S. Mintz, A. Nicosia, N. Bruining, W. Li, C. J. Slager, J. R. T. C. Roelandt, P. W. Serruys, and P. J. de Feyter, "ECG-gated three-dimensional intravascular ultrasound: Feasibility and reproducibility of the automated analysis of coronary lumen and atherosclerotic plaque dimensions in humans," *Circulation* **96**, pp. 2944–2952, Nov. 1997.
3. J. Dijkstra, A. Wahle, G. Koning, J. H. C. Reiber, and M. Sonka, "Quantitative coronary ultrasound: State of the art," in *What's New in Cardiovascular Imaging?*, J. H. C. Reiber and E. E. van der Wall, eds., vol. 204 of *Developments in Cardiovascular Medicine*, pp. 79–94, Kluwer, (Dordrecht), 1998.
4. M. Sonka and X. Zhang, "Assessment of plaque composition using intravascular ultrasound," in *What's New in Cardiovascular Imaging?*, J. H. C. Reiber and E. E. van der Wall, eds., vol. 204 of *Developments in Cardiovascular Medicine*, pp. 183–196, Kluwer, (Dordrecht), 1998.
5. S. P. Wiet, M. J. Vonesh, M. J. Waligora, B. J. Kane, and D. D. McPherson, "The effect of vascular curvature on three-dimensional reconstruction of intravascular ultrasound images," *Annals of Biomedical Engineering* **24**, pp. 695–701, Nov./Dec. 1996.
6. A. Wahle, E. Wellenhofer, I. Mugaragu, H. U. Sauer, H. Oswald, and E. Fleck, "Assessment of diffuse coronary artery disease by quantitative analysis of coronary morphology based upon 3-D reconstruction from biplane angiograms," *IEEE Transactions on Medical Imaging* **14**, pp. 230–241, June 1995.
7. A. Wahle, *Präzise dreidimensionale Rekonstruktion von Gefäßsystemen aus biplanen angiographischen Projektionen und deren klinische Anwendung*, no. 152 in *Fortschritt-Berichte, Reihe Biotechnik (17)*, VDI Verlag, Düsseldorf, 1997. (in German).
8. M. Sonka, X. Zhang, M. Siebes, M. S. Bissing, S. C. DeJong, S. M. Collins, and C. R. McKay, "Segmentation of intravascular ultrasound images: A knowledge-based approach," *IEEE Transactions on Medical Imaging* **14**, pp. 719–732, Dec. 1995.
9. L. Koch, P. Kearney, R. Erbel, T. Roth, J. Ge, R. Brennecke, and J. Meyer, "Three dimensional reconstruction of intracoronary ultrasound images: Roadmapping with simultaneously digitised coronary angiograms," in *Proc. Computers in Cardiology 1993, London UK*, pp. 89–91, IEEE-CS Press, (Los Alamitos CA), 1993.
10. J. L. Evans, K. H. Ng, S. G. Wiet, M. J. Vonesh, W. B. Burns, M. G. Radvany, B. J. Kane, C. J. Davidson, S. I. Roth, B. L. Kramer, S. N. Meyers, and D. D. McPherson, "Accurate three-dimensional reconstruction of intravascular ultrasound data; spatially correct three-dimensional reconstructions," *Circulation* **93**, pp. 567–576, Feb. 1996.
11. S. C. Mitchell, A. Wahle, C. von Birgelen, R. Erbel, and M. Sonka, "Real-time visualization of coronary interventions using VRML," in *Proc. Medical Imaging 1999: Physiology and Function from Multidimensional Images, San Diego CA*, No. 3660-31, SPIE, (Bellingham WA), Feb. 1999.
12. B. O'Neill, *Elementary Differential Geometry*, Academic Press, New York, 1966.
13. G. P. M. Prause, S. C. DeJong, C. R. McKay, and M. Sonka, "Towards a geometrically correct 3-D reconstruction of tortuous coronary arteries based on biplane angiography and intravascular ultrasound," *International Journal of Cardiac Imaging* **13**, pp. 451–462, Dec. 1997.
14. M. Laban, J. A. Oomen, C. J. Slager, J. J. Wentzel, R. Krams, J. C. H. Schuurbiens, A. den Boer, C. von Birgelen, P. W. Serruys, and P. J. de Feyter, "ANGUS: A new approach to three-dimensional reconstruction of coronary vessels by combined use of angiography and intravascular ultrasound," in *Proc. Computers in Cardiology 1995, Vienna AT*, pp. 325–328, IEEE Press, (Piscataway NJ), 1995.
15. R. Shekhar, R. M. Cothren, D. G. Vince, and J. F. Cornhill, "Fusion of intravascular ultrasound and biplane angiography for three-dimensional reconstruction of coronary arteries," in *Proc. Computers in Cardiology 1996, Indianapolis IN*, pp. 5–8, IEEE Press, (Piscataway NJ), 1996.
16. G. P. M. Prause, S. C. DeJong, C. R. McKay, and M. Sonka, "Semi-automated segmentation and 3-D reconstruction of coronary trees: Biplane angiography and intravascular ultrasound data fusion," in *Proc. Medical Imaging 1996: Physiology and Function from Multidimensional Images, Newport Beach CA*, vol. 2709, pp. 82–92, SPIE, (Bellingham WA), 1996.
17. M. Sonka, V. Hlavac, and R. Boyle, *Image Processing, Analysis, and Machine Vision*, PWS Publishing, Pacific Grove, 2nd ed., 1998/99.

18. J. Beier, H. Oswald, H. U. Sauer, and E. Fleck, "Accuracy of measurement in quantitative coronary angiography (QCA)," in *Computer Assisted Radiology (CAR '91)*, H. U. Lemke, M. L. Rhodes, C. C. Jaffe, and R. Felix, eds., pp. 721–726, Springer, (Berlin/New York), 1991.
19. H. Wollschläger, P. Lee, A. Zeiher, U. Solzbach, T. Bonzel, and H. Just, "Mathematical tools for spatial computations with biplane isocentric X-ray equipment," *Biomedizinische Technik* **31**, pp. 101–106, May 1986.
20. S. A. MacKay, M. J. Potel, and J. M. Rubin, "Graphics methods for tracking heart wall motion," *Computers and Biomedical Research* **15**, pp. 455–473, Oct. 1982.
21. L. E. Fencil and C. E. Metz, "Propagation and reduction of error in three-dimensional structure determined from biplane views of unknown orientation," *Medical Physics* **17**, pp. 951–961, Nov./Dec. 1990.
22. K. R. Hoffmann, C. E. Metz, and Y. Chen, "Determination of 3D imaging geometry and object configurations from two biplane views: An enhancement of the Metz-Fencil technique," *Medical Physics* **22**, pp. 1219–1227, Aug. 1995.
23. D. L. Parker, D. L. Pope, R. E. van Bree, and H. W. Marshall, "Three-dimensional reconstruction of moving arterial beds from digital subtraction angiography," *Computers and Biomedical Research* **20**, pp. 166–185, Apr. 1987.
24. A. Wahle, H. Oswald, G. A. Schulze, J. Beier, and E. Fleck, "3-D reconstruction, modelling and viewing of coronary vessels," in *Computer Assisted Radiology (CAR '91)*, H. U. Lemke, M. L. Rhodes, C. C. Jaffe, and R. Felix, eds., pp. 669–676, Springer, (Berlin/New York), 1991.
25. A. Wahle, G. P. M. Prause, S. C. DeJong, and M. Sonka, "Limitations of the manual pullback in intracoronary ultrasound imaging," in *Proc. 20th Annual International Conference of the IEEE Engineering in Medicine and Biology Society (EMBS), Hong Kong*, pp. 506–509, IEEE Press, (Piscataway NJ), 1998. CD-ROM.
26. A. Wahle, G. P. M. Prause, S. C. DeJong, and M. Sonka, "Accurate 3-D fusion of angiographic and intravascular ultrasound data," in *Computer Assisted Radiology and Surgery (CAR '98)*, H. U. Lemke, M. W. Vannier, K. Inamura, and A. G. Farman, eds., vol. 1165 of *Excerpta Medica International Congress Series*, pp. 164–169, Elsevier, (Amsterdam), 1998.
27. A. Wahle, G. P. M. Prause, S. C. DeJong, and M. Sonka, "A comprehensive method for geometrically correct 3-D reconstruction of coronary arteries by fusion of intravascular ultrasound and biplane angiography," in *Proc. First International Workshop for Computer Aided Diagnosis, Chicago IL*, Elsevier, (Amsterdam), Sept. 1998. (in press).
28. A. Wahle, G. P. M. Prause, S. C. DeJong, and M. Sonka, "3-D fusion of biplane angiography and intravascular ultrasound for accurate visualization and volumetry," in *Medical Image Computing and Computer-Assisted Intervention (MICCAI '98)*, W. M. Wells, A. Colchester, and S. Delp, eds., vol. 1496 of *Lecture Notes in Computer Science*, pp. 146–155, Springer, (Berlin/New York), 1998.
29. H. Wollschläger, P. Lee, A. Zeiher, U. Solzbach, T. Bonzel, and H. Just, "Computed triple orthogonal projections for optimal radiological imaging with biplane isocentric multidirectional X-ray systems," in *Proc. Computers in Cardiology 1986, Boston MA*, pp. 185–188, IEEE-CS Press, (Los Alamitos CA), 1986/87.
30. A. C. M. Dumay, J. H. C. Reiber, and J. J. Gerbrands, "Determination of optimal angiographic viewing angles: Basic principles and evaluation study," *IEEE Transactions on Medical Imaging* **13**, pp. 13–24, Mar. 1994.
31. P. M. Hall, "Robust reconstruction of 3-D space-curves from images at arbitrary angles," in *8th British Machine Vision Conference (BMVC '97)*, A. F. Clark, ed., pp. 300–309, BMVA Press, (Essex), 1997.
32. W. Wunderlich, F. Fischer, A. J. Morguet, H. R. Arntz, D. Horstkotte, and H. P. Schultheiss, "Foreshortening display: An on-line method for spatial interpretation and projection assessment of the target coronary segment," in *Proc. Computers in Cardiology 1998, Cleveland OH*, vol. 25, pp. 437–440, IEEE Press, (Piscataway NJ), 1998.
33. U. Solzbach, U. Oser, M. R. Rombach, H. Wollschläger, and H. Just, "Optimum angiographic visualization of coronary segments using computer-aided 3D-reconstruction from biplane views," *Computers and Biomedical Research* **27**, pp. 178–198, June 1994.
34. Y. Sato, T. Araki, M. Hanayama, H. Naito, and S. Tamura, "A viewpoint determination system for stenosis diagnosis and quantification in coronary angiographic image acquisition," *IEEE Transactions on Medical Imaging* **17**, pp. 121–137, Feb. 1998.
35. S. Y. J. Chen and J. D. Carroll, "Computer assisted coronary intervention by use of on-line 3-D reconstruction and optimal view strategy," in *Medical Image Computing and Computer-Assisted Intervention (MICCAI '98)*, W. M. Wells, A. Colchester, and S. Delp, eds., vol. 1496 of *Lecture Notes in Computer Science*, pp. 377–385, Springer, (Berlin/New York), 1998.